Surface Chemistry of Cationic-Ligands-Protected Gold Nanomolecules: Ligand Exchange, Protonation, and Menshutkin Reactions on Au_{25} Cluster

Zhong Huang

Introduction

To date, Au_mSR_n nanoclusters (NCs) have been extensively studied due to their excellent stabilities and intriguing physicochemical properties, such as $Au_{25}(SR)_{18}$, $Au_{38}(SR)_{24}$, $Au_{67}(SR)_{35}$, $Au_{102}(SR)_{44}$, $Au_{130}(SR)_{50}$, and $Au_{144}(SR)_{60}$ can be easily synthesized.[1,2] However, $Au_n(SR)_m$ NCs are mainly prepared through the use of neutral and anionic SR (or acidic ones, which possess the negative charge in solution) ligands, as summarized in Table 1.

Table 1 The summary of SR ligands used for the syntheses of Au NCs with atomic precision.

Types	Thiolate ligands (SR)
Neutral	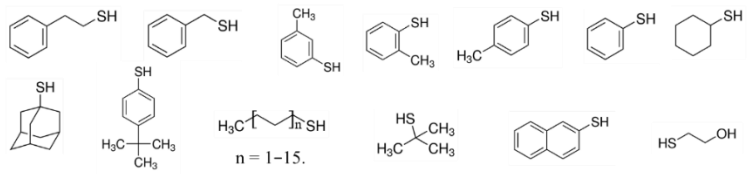 n = 1–15.
Anionic (or acidic)	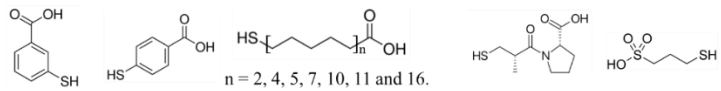 n = 2, 4, 5, 7, 10, 11 and 16.
Cationic (or basic)	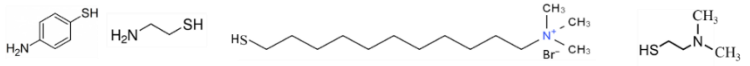
Ones containing both acidic and basic groups	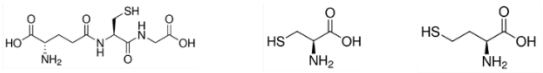

To the best of my knowledge, there are only four reports for the cationic SR (or basic ones, which possess the positive charge in solution). In 2012, Au_{25} NCs stabilized by 4-aminothiophenol ($HSPhNH_2$) was prepared but its molecular formula was accidentally assigned as $Au_{25}(SPhNH_2)_{17}$.[3] Recently, the Xie group developed a NaOH-mediated $NaBH_4$ reduction method for Au_{25} NCs synthesis using cystamine ($HSCH_2CH_2NH_2$). However, cystamine should associate with the mercaptocarboxylic acids for stabilizing Au_{25} NCs. Recently, Ishida et al.[4,5] modified the Burst method at optimized reduction rate, resulting in the successful synthesis of a Au_{25}NCs using a SR ligand with the pendant quaternary-ammonium group ($-[N(CH_3)_3]^+$).The latest reports by the Whetten group[6,7] only reported the evidence of polydisperse captamine ($HS(CH_2)_2N(CH_3)_2$)-protected Au NCs with sizes ranging from 25–144. These few works seem to follow a categorically state mention 2005: "Small positively charged

ligands do not support the production of the monolayer protected clusters (MPCs) in the Brust synthesis." However, in some special areas, such as biological signalling, particle transportation, cellular toxicity, and environmental impact, cationic-ligands-protected NCs can be indispensable due to the good affinity of the cationic ligand for the biomaterial. Accordingly, there is an emergency need for methods to synthesize the cationic-ligand-protected NCs with high-yield and high-purity, and researching their physicochemical properties.

2 Experimental section

2.1 Chemicals

Hydrogen tetrachloroaurate (III) ($HAuCl_4 \cdot 4H_2O$, >99.99%, Wako, Japan), 2-(4-pyridinyl)ethanethiol hydrochloride (4-PyET·HCl, >97%, TCI, Japan), 2-pyridyl ethylmercaptan (2-PyET, TRC, Canada), phenyl ethanethiol (PET, 99%, Wako, Japan), tetra-*n*-octylammonium bromide (TOABr, >98%, Wako, Japan), sodium borohydride ($NaBH_4$, 99%, Wako, Japan), sodium hydroxide (NaOH, >97%, Junsei, Japan), hydrochloric acid (HCl, 35−37%, Kanto, Japan), hydrogen chloride–methanol solution (HCl–MeOH, ~1.25 M, Aldrich), acetic acid (CH_3COOH, >99.7%, Junsei, Japan), deuterium chloride solution (DCl, 35 wt.% in D_2O, Aldrich) and sodium deuteroxide solution (NaOD, 40 wt.% in D_2O, Aldrich) were used as received without further purification. HPLC-grade solvents such as tetrahydrofuran (THF), methanol (MeOH), dimethylformamide (DMF), and dichloromethane (DCM) were purchased from Kanto, Japan. Deionized pure water (>18.2 MΩ) was prepared by an Organo/ELGA purelab system.

2.2 Synthesis and Purification of $Au_{25}(PyET)_{18}$ NCs

Solutions of $HAuCl_4$ (6.7 mM, stock solution) and 4-PyET (100.0 mM, stock solution) were separately prepared with THF and MeOH. In a typical synthesis of $Au_{25}(4\text{-}PyET)_{18}$ NCs, 8 mL of the 4-PyET solution was added dropwise into 24 mL of the $HAuCl_4$ solution (noted the ratio of THF to MeOH was 3:1 by volume, and the ratio of 4-PyET to Au was 5:1 by mole) under stirring. The mixture changed into a light reddish turbid suspension, and then into a white turbid suspension during the addition of 4-PyET. After stirring overnight, white residues were found to stick to the inner wall of the flask (Figure S3.1a, Supporting Information). The white residues could be redispersed completely by sonication for 1 min (Figure S3.1b) to form a turbid suspension again. Then, 1.6 mL of the freshly prepared $NaBH_4$ aqueous solution (1.6 mmol, 10:1 molar ratio of $NaBH_4$ to Au, prepared by dissolving 189.2 mg of $NaBH_4$ in 5 mL of cold pure water) was rapidly added to the suspension under vigorous stirring. The color of the suspension immediately turned black, indicating the formation of Au_m NCs. After approximately 1 h of vigorous stirring, the color became slight brownish (Figure S3.1c). The stirring rate was decreased to 500 rpm and the etching process was allowed to continue for at least 48 h. During the long-time etching process, the solution color slowly changed to dark brown, which suggested that the crude polydisperse Au_m

NCs were converted to monodisperse Au_{25}(4-PyET)$_{18}$ NCs (Figure S3.1d).

The crude sample was cleaned first by centrifugation to remove any solids. Then, under stirring, 2 mL of aqueous HCl (375.0 mM) was rapidly added to the crude sample and the brownish precipitation was collected by centrifugation. The as-collected solid was washed by THF twice and then redissolved in 8 mL of MeOH. The insoluble particles were removed by centrifugation. In 32 mL of the aqueous NaOH solution (200.0 mM), 8 mL of the obtained Au_{25}-containing MeOH solution was added and the Au_{25} NCs then precipitated in water. Finally, the brown solid collected by centrifugation was washed by water thrice to remove impurities and polydisperse Au clusters ([Au(PyET)]$_m$). This final product, [Au_{25}(4-PyET)$_{18}$]$^-$·Na^+ or [Au_{25}(2-PyET)$_{18}$]$^-$·Na^+, was stored in dry form or in a DMF solution. In addition, for comparison, [Au_{25}(PET)$_{18}$]$^-$·TOA^+ NCs were prepared based on a previously reported method.

2.3 Crystallization and X-ray Crystallographic Determination of Au_{25}(PyET)$_{18}$ NCs

Recrystallization of Au_{25}(PyET)$_{18}$ was carried out by a vapor diffusion method. Fully deprotonated Au_{25}(4-PyET)$_{18}$ NCs were dispersed in DMF at a concentration of ~10.0 mg/mL in a 5-mL vial without a seal. The 5-mL vial containing the sample was placed in the middle of a separate 50-mL vial. Then, diethyl ether (non-solvent of NCs) was introduced into the 50-mL vial. After tightly sealing the 50-mL vial, it was kept in a refrigerator at 4 °C. After approximately 5–7 days, black belt-shaped crystals were successfully obtained and analyzed by X-ray diffraction.

2.4 Protonation Reaction on Au_{25}(PyET)$_{18}$ NCs

In 3 mL aliquots of MeOH, each containing 100 μg/mL of Au_{25}(PyET)$_{18}$ NCs, 4.8, 9.6, 14.4, and 28.8 μL of the HCl–MeOH solution (500 mM) were added separately. Each batch was stirred at 300 rpm for 30 s and then subjected to UV-vis absorption characterization in a quartz cuvette with a 10-mm optical path. The reversible protonation–deprotonation process was studied in this part of the experiment by adding 9.6 μL of HCl solution and subsequently 14.4 μL of the NaOH–MeOH solution (500 mM). In NMR monitoring of the protonation, 1.0 mg of Au_{25}(PyET)$_{18}$ NCs was dissolved in 0.6 mL of methanol-d_4, and then 16 μL aliquot of the DCl-D_2O solution (50 mM) was injected step-by-step and immediately analyzed by ^{1}H-NMR. The masses for the free PyET titrations were set equal to those of PyET ligands on the surface of Au_{25}(PyET)$_{18}$ NCs (1.0 mg). The reversible protonation–deprotonation process under NMR investigation was conducted by adding 96 μL of the DCl-D_2O solution and subsequently 144 μL of the NaOD-D_2O solution (50 mM).

2.5 Menshutkin Reaction on Au_{25}(PyET)$_{18}$ NCs

Two-step Menshutkin reaction was investigated in Au_{25}(4-PyET)$_{18}$ cluster. First-step: in 1 mL DMF solvent with 1 mg/mL of Au_{25}(4-PyET)$_{18}$ cluster (~2.4 μmol), liquid Me_2SO_4 (23 μL, ~240 μmol) were added in the mole ratio of Me_2SO_4:4-PyET = 100:1. The mixture was stirred at 500 rpm for different reaction time (5 min, 30 min, 1 h, 2h,

4h and 6 h), and then conducted by UV-vis absorption using a quartz cuvette with a 10-mm optical path. Each batch was first precipitated by dimethyl ether (3 mL), and then washed by DCM (3 mL) twice. The collected samples were vacuum-dried at room temperature for further characterizations. Second-step: the above collected sample (2 h reaction) was redissolved in 1 mL DMF, and another 23 μL of Me_2SO_4 was added for difference reaction time, as same to the case of first-step. Each batch was tested by UV-vis spectra, and then purified for further characterizations.

2.6 Characterization

UV-vis absorption spectra were recorded using a JASCO V-630 spectrophotometer. Electrospray-ionization mass spectrometry (ESI-MS) was performed using a Bruker DaltonicsmicrOTOF-HS mass spectrometer. The purified sample dissolved in methanol (~100 μg/mL) was directly infused at 4 mL·min^{-1}. The nebulizer pressure was set to 1.5 bar, and the sheath gas flow was set to 4.0 L/min. The dry temperature was maintained at 120 °C. The electrospray emitter potential was held at –4500 V (in the negative mode) and 4500 V (in the positive mode). The capillary exit, skimmer 1, hexapole 1, and skimmer 2 voltages were 200, 50, 25, and 28 V, respectively. The lens 1 transfer and lens 1 pre plus storage were set at 160 and 30 μs, respectively. Thermogravimetric analysis (TGA) was undertaken on a Shimadzu DTG-60H instrument in a N_2 atmosphere (flow rate: ~100 mL min^{-1}). The obtained pure $[Au_{25}(PyET)_{18}]^{-}\cdot Na^{+}$ was put into an alumina cell, and the temperature was increased to 600 °C at a heating rate of 5 °C min^{-1}. ^{1}H-NMR and COSY analyses were performed on a JMTC-400/54/SS (JEOL) spectrometer operating at 400 MHz.

3 Results and discussions

3.1 Kinetics of the Cationic-Ligand-Exchange Reaction

Figure 1 displays the pseudo-first-order rate plot. The reaction can be analyzed as a biphasic process; a rapid first-order process (–0.0043 min^{-1}, Phase I) which transitions to a slower process (–0.0026 min^{-1}, Phase II). These results indicate that the cationic-ligand-exchange process is different to those previously reported for neutral-thiol-to-neutral-thiol ligand exchanges on Au_{25}, in which the kinetic rate is constant under the similar experimental conditions of the two thiolate ligands at room temperature.

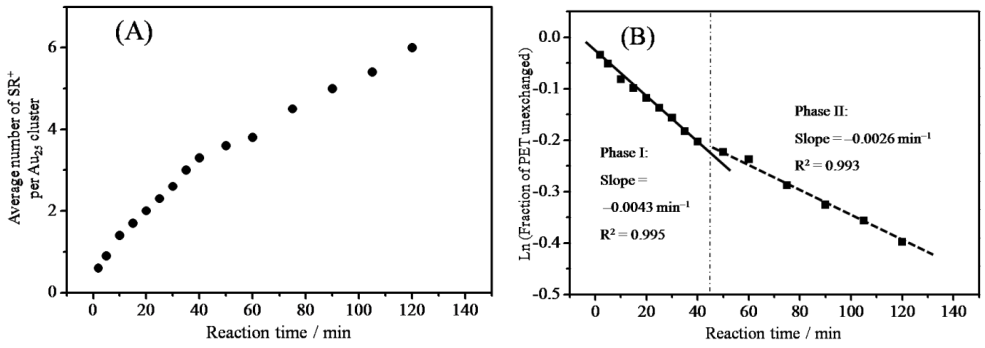

Figure 1 (A) Average number of SR^+ ligands per cluster (max: 18) on the cluster

surface during the ligand-exchange reaction as determined by ^{1}H-NMR spectroscopy. (B) Ln(Fraction of unexchanged PET on the cluster surface) for the ligand-exchange reaction with SR^+ as a function of reaction time. The two lines in (b) are the lines of best fit at 0–40 min (Phase I) and 50–120 min (Phase II), respectively.

There are two types of coulombic repulsions that operate in the current system, namely (i) between the surface SR^+ and the free SR^+ in solution, and (ii) among the SR^+ ligands on the cluster surface, as shown in Figure 2. In the first case (i), when a PET on the cluster surface becomes detached with the concomitant coupling of SR^+ to the Au_{25} surface, repulsions between the attached SR^+ and those free in solution hinder further ligand exchange, as observed by the significant decrease in reaction rate during Phase II of the reaction (Figure 1) and the non-binomial distribution of $Au_{25}(PET)_{18-x}(SR^+)_x$ at times in excess of 30 min. In the second case (ii), cationic groups densely populated on the surface of a Au_{25} cluster experience strong coulombic repulsions. A higher number of cationic ligands strongly decreases the thermal stability of the Au_{25}structure, consistent with my lab's previous TG-DTA data that indicate that a fully cationized $Au_{25}(SR^+)_{18}$ cluster exhibits a lower decomposition temperature. Similar ligand-induced instability was also reported for anionic $Au_{25}(S(CH_2)_nCOOH)_{18}$ nanoclusters.

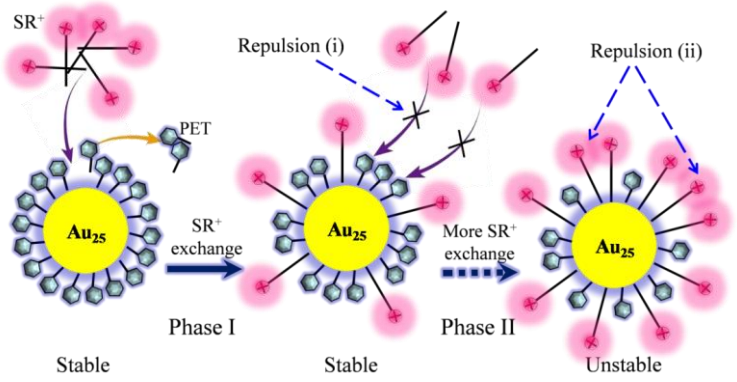

Figure 2 Schematic representation of various coulombic repulsions during cationic-ligand exchange: (i) between the surface SR^+ and the free SR^+ in solution, and (ii) between the SR^+ ligands on the cluster surface (PET: 2-phenylethanethiol; SR^+: (11-mercaptoundecyl)-*N*,*N*,*N*-trimethylammonium).

3.2 Synthesis and Characterization of $Au_{25}(PyET)_{18}$ NCs

As shown in Figure 3, the UV-vis absorption spectra of the as-purified products both showed three distinct absorption bands at ~670, 450, and 400 nm and two weak absorption bands at ~560 and 780 nm (Figures 3A and C), which represent the typical spectroscopic fingerprints of SR-protected Au_{25} NCs with a core charge of −1. Negative-mode ESI-MS of the purified products showed only one peak at *m/z* ~7411.97, corresponding to $[Au_{25}(PyET)_{18}]^-$, for both 4-PyET and 2-PyET. The charge state (−1) of Au_{25} NCs was confirmed by the characteristic peak separations of *m/z* ~1.00 and the molecular formula of $Au_{25}(PyET)_{18}$ was validated by matching the observed isotopic patterns with the simulated ones (Figures 3B and D). Moreover, the positive-mode ESI-

MS of both $Au_{25}(4\text{-PyET})_{18}$ and $Au_{25}(2\text{-PyET})_{18}$ NCs detected predominant peaks of $[Au_{25}(PyET)_{18}Na_x]^{x-1}$, suggesting the counterions of Au_{25} NCs should be Na^+ cations, which may coordinate strongly to pendant Py-groups via the N-atom's long pair of electrons. TGA revealed weight losses of ~33.9% and ~33.7% for $[Au_{25}(4\text{-PyET})_{18}]^-\cdot Na^+$ and $[Au_{25}(2\text{-PyET})_{18}]^-\cdot Na^+$, respectively, which are both very close to the theoretical loss of 33.8%. The yields of the final $Au_{25}(4\text{-PyET})_{18}$ and $Au_{25}(2\text{-PyET})_{18}$ NCs were calculated to be ~30% and ~35%, respectively, on the basis of Au atom content.

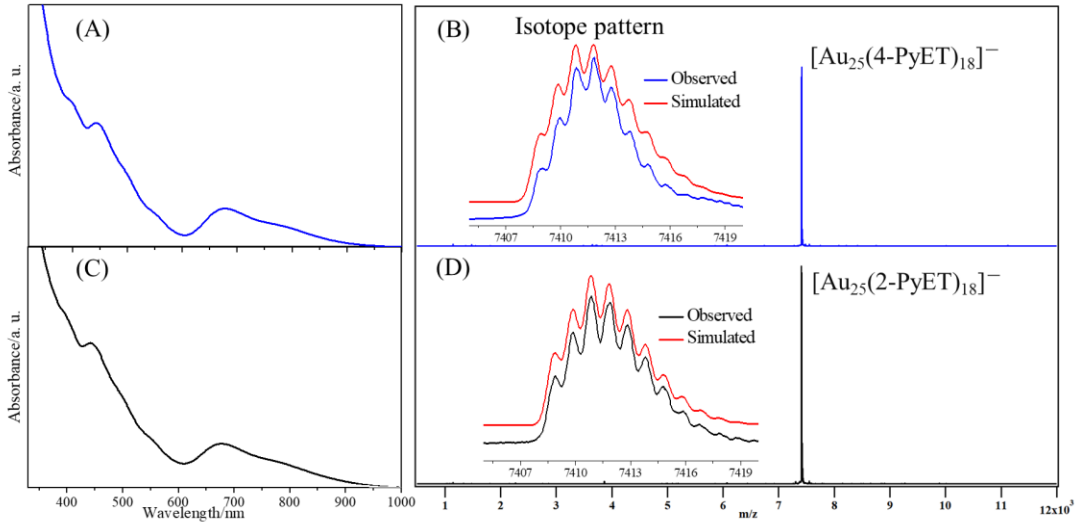

Figure 3 UV-vis absorption and negative-mode ESI mass spectra of purified $Au_{25}(PyET)_{18}$ NCs: (A, B) $[Au_{25}(4\text{-PyET})_{18}]^-$ and (C, D) $[Au_{25}(2\text{-PyET})_{18}]^-$ (The insets show corresponding isotope patterns for the observed and simulated spectra).

3.3 Photoluminescence of $Au_{25}(SR)_{18}$ NCs

The excitation spectra of $Au_{25}(SR)_{18}$ all shows two board peaks at ~ 365 and ~ 624 nm, which both emit the maximal PL at ~ 719 nm. Because under 624 nm excitation, the weak broad PL peaks (~ 719 nm) would overlap with the strong incident wavelength (624 nm), it was hard to compare the PL emissions among the as-measured samples. So here, the PL test were all carried out under the excitation wavelength at 365 nm.

Under the same conditions, the PL tests of $Au_{25}(PET)_{18}$ and $Au_{25}(PyET)_{18}$ NCs (noting that the counterion was tetra-*n*-octylammonium TOA^+ for the former, and Na^+ for the latter) were conducted and compared, as shown in Figure 4. The $Au_{25}(PET)_{18}$ was found to exhibit weak emission at ~719 nm under the 365 nm excitation. By contrast, the emission wavelength (~719 nm) of $Au_{25}(4\text{-PyET})_{18}$ or $Au_{25}(2\text{-PyET})_{18}$ remained constant whereas the PL intensities showed the definite enhancements. The fluorescence intensity follows the order $Au_{25}(4\text{-PyET})_{18}$ > $Au_{25}(2\text{-PyET})_{18}$ > $Au_{25}(PET)_{18}$. Especially in the $Au_{25}(4\text{-PyET})_{18}$, which was ~6-fold greater than that of the $Au_{25}(PET)_{18}$. Notably, use of difference solvents required a collection by the refractive index of two solvents (for MeOH and toluene, 1.329 and 1.49, respectively), however it is clear that the PL of PyET cases are stronger than that of PET. Since the

$Au_{25}(SR)_{18}$ NCs have the common structure, an icosahedral Au_{13} core that is capped by three pairs of $Au_2(SR)_3$ staple motifs (Scheme 4.1), the above observation indicated that the surface ligands play an important role in the PL emission, that is, SR ligands with pyridyl-group can enhance the PL of Au_{25} NCs over that with phenyl-group.

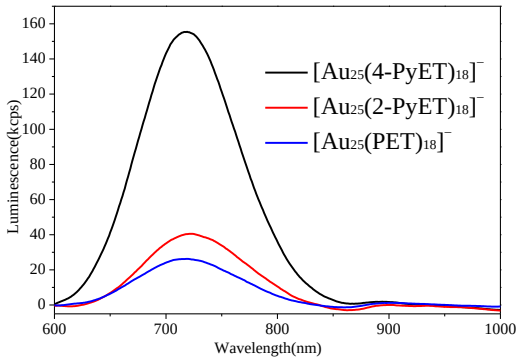

Figure 4 Photoluminescence spectra of (a) $Au_{25}(SR)_{18}$ with different aromatic rings (PET, 4-PyET and 2-PyET). (Solvents: toluene for PET case, and MeOH for PyET cases; excitation: 365 nm; solution concentration: 100 μg/mL).

3.4 Menshutkin Reaction of $Au_{25}(SR)_{18}$ NCs

In 1.0 mL Au_{25}(4-PyET)$_{18}$-DMF solution (1.0 mg/mL), dimethyl sulfate (Me_2SO_4, 23 μL, which is 100 times as high as the mole ratio of surface 4-PyET ligands) was added, and the process was firstly monitored by UV-vis absorption spectroscopy. As presented in Figure 5a, the characteristic absorption peaks of Au_{25} cluster at ~400 and 560 nm had a slight increase, whereas the peaks at ~450, 670 and 780 nm showed a slight decrease in 60 min reaction. Interestingly, such absorption changes were also observed when the Au_{25}(4-PyET)$_{18}$ cluster was treated with H^+, in which a reversible protonation of Py-group gives its positive form, $-C_5H_4NH^+$. These results indicate that the geometric structure of Au_{25}(4-PyET)$_{18}$ cluster might have a slight distortion, caused by the surface charge anisotropy when the positive charges (H^+ or $[N-CH_3]^+$ in present work) were distributed on the surface of Au_{25} cluster. This indicated that the surface 4-PyET ligands were methylated on Py-group through the Menshutkin reaction. Further increasing the reaction to 120 min and 240 min, the absorption peaks show the negligible change, suggesting the good stability of the methylated (or cationized) Au_{25} clusters.

Since the initial $[Au_{25}(4\text{-PyET})_{18}]^-$ is negatively charged, I first monitored the time course of the Menshutkin reaction by negative-mode ESI-MS. In the starting, only one peak located at ~7411.97 *m/z* was observed in the spectrum of the initial compound, which corresponds to the starting $[Au_{25}(4\text{-PyET})_{18}]^-$. Following the Menshukin reaction, only after 5 min reaction, the starting$[Au_{25}(4\text{-PyET})_{18}]^-$ clusters disappeared, instead of the resulting cationized clusters, $[Au^{-1}{}_{25}(4\text{-PyET}{-}CH_3^+)_x(4\text{-PyET})_{18-x}(MeSO_4^-)_{x+1}]^{2-}$ ($2 \leq x \leq 17$), were observed by negative-mode ESI-MS. This indicated that all initial Au_{25}clusters had been consumed in a very short time of 5 min.

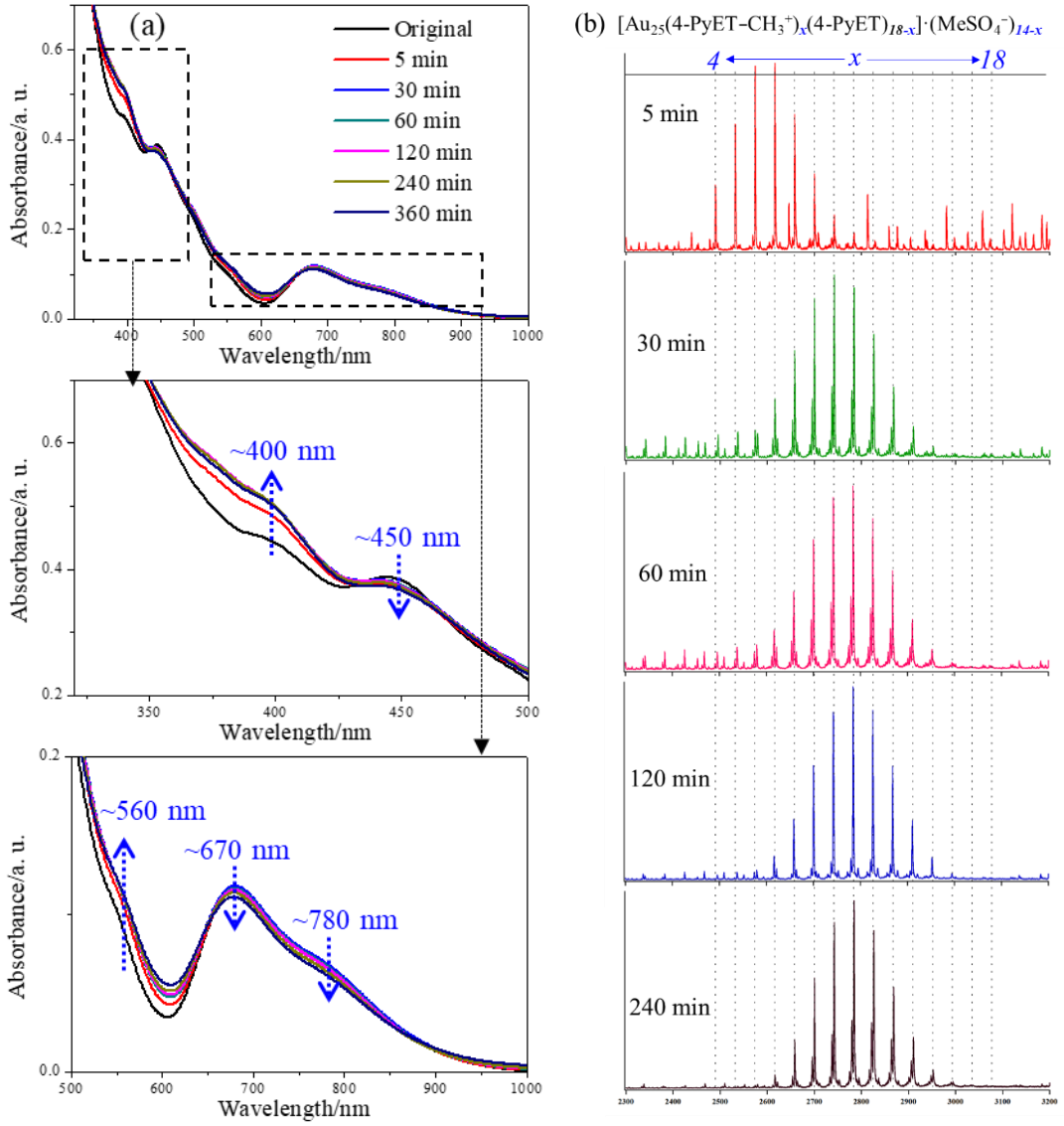

Figure 5 (a) UV−vis absorption and (b) positive-mode ESI mass spectra of group III (2300−3200 m/z) of samples collected at different times during first-step Menshutkin reaction.

Figure 5b displays positive-mode ESI-MS of the sample after Menshutkin reaction of different time (5, 30, 60 120 and 240 min).The full spectrum in Figure S5.4a displays prominent groups of peaks for +2 (group II, 3500–4700*m/z*), +2 (group III, 2300–3200 *m/z*), and +3 (group IV, 1800–2300 *m/z*) charged states; the corresponding detailed assignments are presented in Table S2–4, respectively. Figure 5b, as an example, shows the *x* value of the cationized Au_{25} clusters with +3 charge state. The cationized Au_{25} clusters, $[Au^{-1}_{25}(4\text{-PyET}{-}CH_3^+)_x(4\text{-PyET})_{18-x}(MeSO_4^-)_y]^{3+}$ ($4 \le x \le 18$, $y = x–1$) were successfully characterized by positive-mode ESI-MS. After 5 min reaction, the *x* was distributed between 4 and 12. When increasing the reaction time to 30, 60 and120 min, *x* values were observed to increase: *x* = 4–15, 5–16, and 7–16, respectively, suggesting the extent of Menshutkin reaction would proceed along the reaction time. Further prolonging the reaction time to 240 min, the *x* value still ranges from 7 to 16. Based on

these, it can be concluded that through Menshutkin reaction, the surface 4-PyET of Au_{25} clusters can be easily methylated into cationic 4-PyET−CH_3^+, which is a facile way to the consistently-cationized Au_{25} clusters.

4. Conclusions

Surface chemistry on cationic-ligands-protected metal clusters of atomically-precision is rarely reported, but providing a new platform for the functionalization of clusters toward enhancing their practical utility. In this thesis, taking the $Au_{25}(SR)_{18}$ cluster as the example, three interfacial surface reactions: ligand-exchange, protonation and Menshutkin reactions, have been investigated on the cationic-ligands-protected noble metal clusters. The key results and conclusions can be summarized as follows:

1) the kinetics of the cationic-ligand-exchange reactions of Au_{25} nanoclusters, which is different from a typical neutral-thiol-to-neutral-thiol ligand exchange, is strongly dependent on how the SR^+ ligands interact with each other during the ligand-exchange process.

2) High-purity and high-yield Au_{25} clusters protected by the basic pyridyl ethanethiol ($HSCH_2CH_2Py$, 4-PyET and 2-PyET) were prepared using a simple one-pot synthetic strategy. Single crystal of $[Au_{25}(4\text{-PyET})_{18}]^-\cdot Na^+$ was successfully prepared and its structure solved. It reveals a structure similar to that known for the phenyl ethanethiolate analog, but with pyridyl-N coordination to Na^+, a more relaxed ligand shell, and a profoundly layered arrangement in the solid state. $Au_{25}(PyET)_{18}$ clusters being endowed with a unique (de)protonation equilibria, can conjugate to H^+ through the pendant Py moiety, similar to a heterocyclic base.

3) Even only one element difference between $Au_{25}(PyET)_{18}$ and $Au_{25}(PET)_{18}$ clusters, the Py moieties plays a major role in the PL efficiency. The result indicated that Py groups on cluster surface donate more electrons to Au_{25} core, resulting in the enhanced PL emissions of $Au_{25}(PyET)_{18}$ clusters. The resonance-coupled structure of PyET ligands, caused by proton (H^+), would hinder the electron donation, and quench the emission of Au_{25} NCs.

3) Menshutkin reaction of surface 4-PyET ligands on $Au_{25}(4\text{-PyET})_{18}$ clusters was investigated for the first time. The incorporation of a reactive Py group amenable to be methylated can easily transform the neutral PyET-capped metal clusters into the cationized ones.

References

(1) Jin, R.; Zeng, C.; Zhou, M.; Chen, Y. Atomically precise colloidal metal nanoclusters and nanoparticles: fundamentals and opportunities. *Chem. Rev.* **2016**,*116*, 10346–10413.

(2) Chakraborty, I.; Pradeep, T. Atomically Precise Clusters of Noble Metals: Emerging Link between Atoms and Nanoparticles. *Chem. Rev.***2017**, *117*, 8208–8271.

(3) Lavenn, C.; Albrieux, F.; Bergeret, G.; Chiriac, R.; Delichere, P.; Tuel, A.; Demessence, A. Functionalized gold magic clusters: $Au_{25}(SPhNH_2)_{17}$. *Nanoscale* **2012**. *4*, 7334–7337.

(4) Ishida, Y.; Narita, K.; Yonezawa, T.; Whetten, R. L. Fully cationized goldclusters: synthesis of $Au_{25}(SR^{+})_{18}$. *J. Phys. Chem. Lett.* **2016**, *7*, 3718–3722.

(5) Ishida, Y.; Huang, Y. L.; Yonezawa, T.; Narita, K. Charge neutralization strategy: a novel synthetic approach to fully cationized thiolate−protected $Au_{25}(SR^{+})_{18}$ clusters with atomic precision. *ChemNanoMat* **2017**, *3*, 298−302.

(6) Hoque, M. M.; Black, D. M.; Mayer, K. M.; Dass, A.; Whetten, R. L. The base side of noble metal clusters: efficient route to captamino-gold, $Au_n(-S(CH_2)_2N(CH_3)_2)_p$, n= 25–144. *J. Phys. Chem. Lett.* **2019,** *10***,** 3307−3311.

(7) Hoque, M. M.; Dass, A.; Mayer, K. M.; Whetten, R. L. Protein-like large gold clusters based on the ω-amino-thiolate DMAET: precision thermal and reaction control leads to selective formation of cationic gold clusters in the critical size range, n= 130–144 Au atoms. *J. Phys. Chem. C* **2019**, *123*, 14871–14879.